Heat and Mass Transfer (2023) 59:21–37
https://doi.org/10.1007/s00231-022-03231-0

ORIGINAL ARTICLE

Numerical investigation and mechanism analysis of heat transfer enhancement in a helical tube by square wave pulsating flow

Yaxia Li[1] · Qingping Yu[1] · Sanchuan Yu[1] · Ping Zhang[1] · Jing Zhang[1,2]

Received: 8 October 2021 / Accepted: 25 April 2022 / Published online: 18 May 2022
© The Author(s), under exclusive licence to Springer-Verlag GmbH Germany, part of Springer Nature 2022

Abstract
In this paper, heat transfer enhancement of square wave pulsating flow in a helical tube is numerically investigated. The numerical results are in good agreement with the experimental results. Related parameters of square wave pulsating flow including dimensionless frequency Wo number and dimensionless amplitude $\overline{A}$ have been researched in detailed. The heat transfer enhancement mechanism of square wave pulsating flow in helical tubes has been revealed. And the influence of fluid properties on heat transfer enhancement has also been discussed. The results show that both Nusselt number Nu and flow resistance coefficient f_{D} increase with the enhancement of $\overline{A}$ and Wo values. The square wave pulsating flow of $Wo=9$ and $\overline{A}=0.25$ performs best in comprehensive heat transfer enhancement within the studied range. Comprehensive enhancement heat transfer factor TP is between $1.03 \sim 1.12$. The increases of secondary flow and turbulence intensity as well as the emergence of backflow near the inner wall due to the flow rate sudden change both contribute to heat transfer enhancement. Local Nusselt number Nu_{local} of the inner wall in the pulsating state is up to 7.35% higher than that in the steady state when the medium is water. In the helical tube, the square wave pulsating flow is more suitable to enhance heat transfer of fluid with small Prandtl number.

Nomenclature

A	Pulsating amplitude, m/s
$\overline{A}$	Dimensionless amplitude
c_p	Specific heat, kJ/kg·K
d	Tube diameter, mm
D	Helical diameter, mm
f_D	Flow resistance coefficient
f	Frequency,Hz
h	Heat transfer coefficient,W/m^2·K
k	Thermal conductivity, W/m·K
L	Length of helical tube, mm
p	Pressure, Pa
P_c	Coil pitch, mm
q	Heat flux, W/m^2
t	Time, s
$\overline{t}$	Dimensionless time
T	Temperature, K
v	Velocity, m/s

Greek symbols

α	Angle, radian
β	The duty ratio of the square wave
Γ	Period of the pulsation, s
μ	Viscosity, Pa·s
υ	Kinematic viscosity,m^2/s
ρ	Density, kg/m^3
$\triangle p$	Pressure drop,Pa

Subscripts

f	Fluid
in	Inlet
m	Mean
p	Pulsating flow

Highlights
- Square wave pulsating flow can improve the heat transfer performance of the helical tube.
- TP is 1.12 at the optimum pulsation condition $Wo=9$ and $\overline{A}=0.25$.
- The heat transfer enhancing mechanism of square wave pulsating flow in helical tube were explored.
- Influence of Pr number on heat transfer enhancement of pulsating flow in helical tube was studied.

✉ Yaxia Li
liyaxia@syuct.edu.cn

1 School of Mechanical and Power Engineering, Shenyang University of Chemical Technology, Shenyang 110142, China

2 School of Chemical Engineering & Technology, Tianjin University, Tianjin 300350, China

s Steady flow
w Wall

Dimensionless numbers

De Dean number
Nu Nusselt number
Pr Prandtl number
Re Reynolds number
Wo Womersley number

1 Introduction

Helical tube has a broad range of application in various industry devices such as heat exchangers, chemical reactors, steam generators and mixing vessels [1]. It has the advantages of compact structure and high heat exchange efficiency [2, 3]. The study on fluid flow characteristic and heat transfer mechanism in helical tubes is always a hot issue in the last several decades. A large number of literatures have reported the researches on fluid flow characteristic, heat transfer performance and compound enhanced heat transfer in helical tubes by using experimental or numerical methods. The main parameters affecting the heat transfer efficiency of helical tube include curvature and torsion of the tube, flow parameter characterized by Reynolds number or Dean number as well as properties of fluids. The high heat transfer efficiency of the helical tube is mainly due to the self-generated secondary flow under the action of centrifugal force. Yang et al. [4, 5] discussed the effects of the Dean number, torsion, and Prandtl number of fluid on the convective heat transfer in helical tubes. It was concluded that the secondary flow would become stronger when the Dean number increases. As the torsion increased, the temperature distribution in the cross-section was asymmetrical. Khoshvaght-Aliabadi [6] analyzed the thermal–hydraulic performance in the helical tube for different working fluids. They found that the Nusselt number increased with Prandtl number increasing, but the friction coefficient changed little. Based on different helical tube structural parameters and different fluids, El-Genk [7] proposed correlations of flow resistance coefficient and Nusselt number by handling the experimental data reported in the literatures. Hardik et al. [8] analyzed the local heat transfer performance in a helical tube. The results showed that values of Nusselt number of the outer wall were greater than those of the inner wall. Li et al. [9] and Zhang et al. [10] analyzed the field synergy of the velocity and temperature fields in helical tubes with semicircular and rectangular cross sections. They proposed that heat transfer efficiency of helical tubes could be further enhanced by improving the secondary flow fields near the inner wall.

At present, some passive and active heat transfer enhancement methods have been applied to helical tubes. The mechanism of heat transfer enhancement is to increase the intensity of fluid turbulence and improve the characteristics of secondary flow fields. The passive method includes changing the tube wall characteristics or installing disturbance elements. Li et al. [11] and Zachár et al. [12] numerically studied the heat transfer enhancing performance by adding spiral corrugation on the inner wall of helical tube, respectively. Conclusions were drawn that heat transfer performance could be improved to a certain extent, however, the flow resistance would increase significantly at the same time. And Rainieri et al. [13, 14] pointed out that this method was more suitable for the high Reynolds number. In recent literatures [15–18], researches on installing disturbance element in helical tube to enhance heat transfer have also been reported, such as spiral coils or vortex generators. The disadvantage of placing a spiral coil in a helical tube to achieve heat transfer enhancement is that the flow resistance increases significantly. The vortex generator can enhance heat transfer by changing the flow field characteristics near the wall, but the number and location of installation are easy to be limited.

In addition to the above passive methods, active enhanced heat transfer method is also applied to helical tubes. Pulsating flow is one of the effective active methods. Some experimental and numerical studies have been carried out to study pulsating flow in helical tubes. Sinusoidal and square wave are two common used patterns of pulsation. Many researches on heat transfer enhancement of sinusoidal pulsating flow in helical tubes have been reported in the literatures. The main affecting factors are Reynolds number, pulsating frequency and pulsating amplitude [19, 20]. Rabadi et al. [21] pointed out that heat transfer efficiency might be even reduced at some specific frequency and amplitude of sinusoidal wave pulsating flow in the curved tube. Pan et al. [22, 23] revealed the mechanism of sinusoidal pulsating flow enhancing heat transfer in helical tubes based on the field synergy principle. The results showed that volume average field synergy angle under the pulsating flow was less 2.45% than that under the steady flow. Kharvani et al. [24, 25] considered that the upstream pulsation heat transfer coefficient was larger than the downstream pulsation in helical tubes. For larger mean Reynolds numbers, the relative average heat transfer coefficient was increased by 16–26%. Guo et al. [26] simulated nanofluids heat transfer in a helical coil under pulsation condition. They found the secondary flow generated in the cross section and the counter-rotating vortex formed in the axial direction both devoted to the heat transfer augmentation under pulsating state.

Compared with the sinusoidal wave, there is a drastic change of velocity in square wave. According to reference [27], many scholars pointed out that square wave pulsating flow significantly enhanced heat transfer. Zhang et al. [28] pointed out that square wave pulsating flow caused greater disturbance to the fluid and promoted the mixing of fluids more easily. Thus it might be more virtue for heat transfer enhancement. In addition, square wave pulsating flow is easy to achieve. However, the study on square wave pulsating flow in helical tube is rare, except that Hamed et al. [29] carried out the experimental study. They investigated heat transfer and pressure drop of square wave pulsating flow in helical coiled tube at the condition of constant heat flux. The results revealed that increment in pressure drop was nearly 3–7% in pulsating flow compared to the steady one, while convective heat transfer was enhanced up to 39%.

According to the literature reviews, it can be found that the research on the flow field and heat transfer characteristics of the square wave pulsating flow in the helical tube is not deep enough. Its mechanism of heat transfer enhancement is not clear. In addition, the research of the fluids properties affecting on pulsating flow enhancing heat transfer in helical tubes has not been found. For the above reasons, the paper has studied the heat transfer enhancing characteristics of the square wave pulsating flow in the helical tube using the numerical method. The influences of the dimensionless frequency and dimensionless amplitude of the square wave pulsating flow on heat transfer enhancement have been investigated in detail based on the boundary condition of constant wall temperature. The distribution of flow field, temperature field and local heat transfer characteristics in a pulsating period is analyzed in detail. Based on these, heat transfer enhancing mechanism of square wave pulsating flow in helical tube has been revealed. In addition, the influence of the Prandtl number of working fluids on the heat transfer enhancing for pulsating flow in the helical tube has also been studied.

2 Numerical simulation

2.1 Physical and mathematical models

In the present study, the helical tube with a circular cross section is vertically oriented, seen in Fig. 1. The number of turns

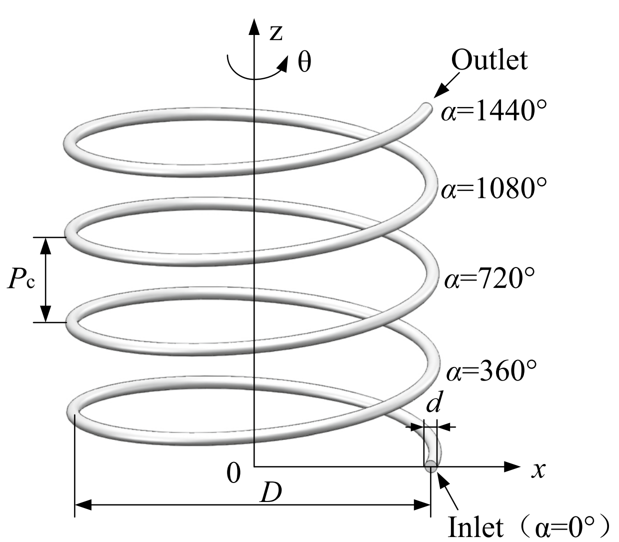

Fig. 1 Basic geometry of the helical tube

Table 1 Geometric parameters of helical tube

Parameters	Dimensions
Number of coil turns	4
Inner diameter of circular tube (mm)	7.5
Helical diameter (mm)	218
Pitch of helical tube (mm)	55
Length of helical tube (mm)	2748

of the helical tube is set as 4, namely the angle $\alpha = 1440°$. The helical diameter and the pitch of the helical tube are represented by D and P_c respectively. The inner diameter of the circular tube is characterized by d. The geometric parameters of the helical tube have been listed in Table 1.

The fluid domain is three-dimensional, incompressible and unsteady. Water is used as working fluid. The governing equations including continuity, momentum and energy equations for the fluid domain can be expressed as follows [26]:

Continuity equation:

$$\nabla \cdot \left(\rho\vec{v}\right)=0 \tag{1}$$

Momentum equation:

$$\frac{\rho\partial\vec{v}}{\partial t} + \rho(\vec{v} \cdot \nabla\vec{v}) = -\nabla p + \mu\nabla^2\vec{v} \tag{2}$$

Energy equation:

$$\rho c_p \frac{\partial T}{\partial t} + \rho c_p \vec{v} \cdot \nabla T = \nabla \cdot [k(\nabla T)] \tag{3}$$

where ρ is density, p is pressure, μ is viscosity, c_p is specific heat, T is temperature, t is the time and k is thermal conductivity.

Details of the boundary conditions are given as follows: At the inlet, the inlet velocity v_{in} and inlet temperature T_{in} are set to be uniformly distributed with $T_{in} = 293$ K. A square wave pulsation displayed in Fig. 2 is used to describe the changing of v_{in} and its mathematical expression is given in Eq. (4).

$$v_{in} = \begin{cases} v_m + A & n\Gamma < t \le (n+1-\beta) \\ v_m - A & (n+\beta)\Gamma < t \le (n+1)\Gamma \end{cases} \quad n = 0, 1, 2, .. \tag{4}$$

Here, Γ is the period of the square wave pulsation and n is the natural number. v_m is the average velocity in a pulsating period. A is the amplitude of square wave pulsating flow. It is the velocity difference between extreme velocity (v_{max} or v_{min}) and average velocity v_m. v_{max} and v_{min} are respectively the maximum and minimum velocity in the helical tube at pulsating state. $\beta = \Delta t/\Gamma$ is defined as the duty ratio of the square wave and used to characterize the proportion of the maximum velocity time length Δt in a pulsating period. $\beta = 0.5$ is selected in the present study. The inlet velocity is guided by

Fig. 2 The pattern of pulsation inlet velocity

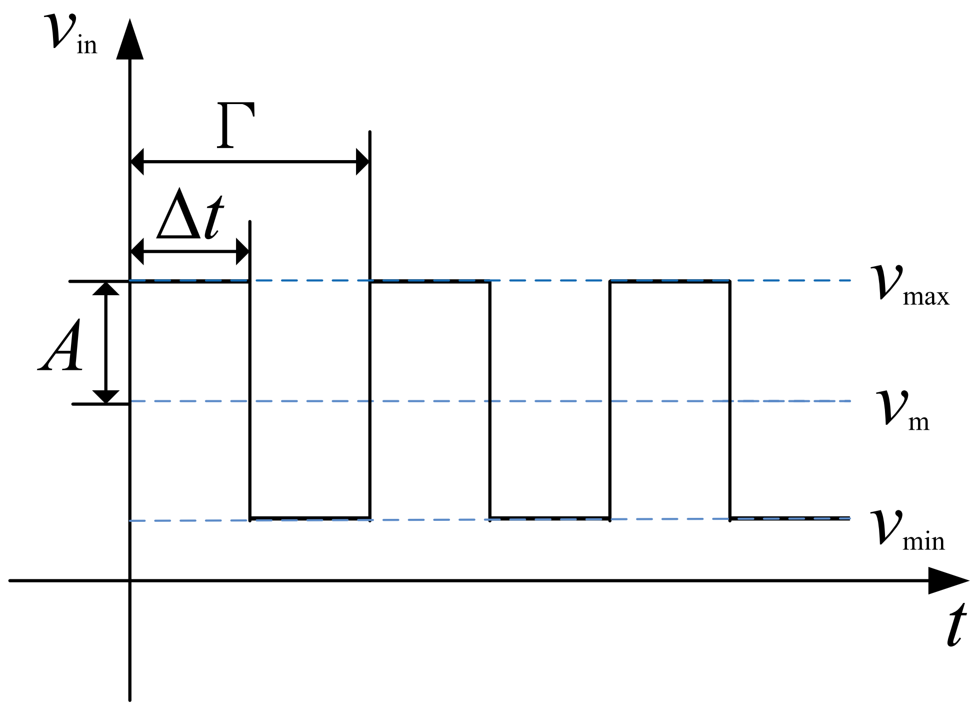

the user-defined functions (UDF) of the CFD software in the present study.

At the outlet, the pressure outlet boundary condition is adopted and the relative pressure of outlet is set as zero. The no-slip and uniform wall temperature boundary conditions are imposed on the wall, where the value of wall temperature T_w is set as $T_w = 343$ K. The initial condition is that the initial fluid velocity and temperature is taken as the mean velocity and mean temperature at the inlet. The inlet thermo-physical properties of water are displayed in Table 2 at room temperature of 293 K [6].

2.2 Main parameter definition

Dimensionless parameter Dean number *De* is used to characterize the flow of fluids in helical tube and is expressed as [30]:

$$De = Re\sqrt{d/D} \tag{5}$$

where, *Re* is the Reynolds number and is defined as:

$$Re = \frac{\rho v_m d}{\mu} \tag{6}$$

The dimensionless amplitude $\overline{A}$ and dimensionless frequency *Wo* are used to characterize the pulsating flow and are defined respectively as follows:

$$\overline{A} = \frac{A}{v_m} \tag{7}$$

$$Wo = \frac{d}{2}\sqrt{\frac{2\pi f}{\upsilon}} \tag{8}$$

where, $f = 1/\Gamma$ is pulsating frequency and υ is the kinematic viscosity of the fluid. In the present study, the value of f ranges from 0.125 Hz to 8 Hz to obtain good heat transfer enhancement effect. At the same time, the value of f should be taken into account that the value of Γ is an integer.

The dimensionless time $\overline{t}$ is expressed as:

$$\overline{t} = t/\Gamma \tag{9}$$

The average Nusselt number *Nu* and flow resistance coefficient f_D are defined as follows:

$$Nu = \frac{hd}{k} \tag{10}$$

Table 2 Thermo-physical properties of working fluids

Property Coolant	Density (kgm^{-3})	Dynamic viscosity ($kgm^{-1}\ s^{-1}$)	Heat capacity ($Jkg^{-1}\ K^{-1}$)	Thermal conductivity ($Wm^{-1}\ K^{-1}$)	Prandtl number
Water	998.2	1.003×10^{-3}	4182	0.606	6.92

$$f_D = \frac{2d\Delta p}{\rho v_{\mathrm{m}}^2 L} \tag{11}$$

where, L is the length of the helical tube. h is average heat transfer coefficient and Δp is average pressure drop calculated by [22]:

$$h = \frac{1/t\int_0^t q dt}{1/t\int_0^t (T_{\mathrm{w}} - T_{\mathrm{f}})dt} \tag{12}$$

$$\Delta p = 1/t\int_0^t \Delta p dt \tag{13}$$

where, q is heat flux, T_{f} is the temperature of working fluid, T_{w} is the wall temperature.

2.3 Numerical simulation method

The commercial CFD code ANSYS Fluent 16.2 is used for the numerical solution. Unsteady segregated solver is used to handle Navier–Stokes equations and energy equations by finite volume method. The realizable k-ε turbulent model [31] is employed for it has the superior performance in deal with the flows involving rotation, great reverse pressure gradient and back flow. The PISO algorithm [23] is utilized to deal with the coupling of pressure and velocity. The convective term in momentum and energy equations are discretized by a second-order upwind scheme. And the time discretization adopts a second order accurate fully implicit scheme. For all simulations, the computations are considered to be converged when the residuals of continuity equations are less than 10^{-4} and the momentum and energy equation are less than 10^{-6}. Computers with 3.3 GHz processor and 8.0 GB RAM are used. It takes about 12 h to obtain the calculation results at the specific amplitude, frequency and velocity.

2.4 Grid and time step validation

In order to ensure the accuracy of the calculation results, the independence of the calculation grid and time step has been verified. The calculation zones are discretized with structured hexahedral grid, and local grid refinement is applied in the boundary layer. Figure 3 presents grids of the cross section. The standard wall function method is used for the near wall region. The wall y plus is evaluated to check the requirement of standard wall function. Four sets of grid system with gradually increasing grid number are generated to valid the influence of grid on the numerical results and they are Grid 1 (1,111,808), Grid 2 (1,389,760), Grid 3 (1,516,352) and Grid 4 (1,683,856). The values of f_{D} and Nu calculated based on the four sets of grid system are displayed in Table 3. It can be found that relative deviation of f_{D} and

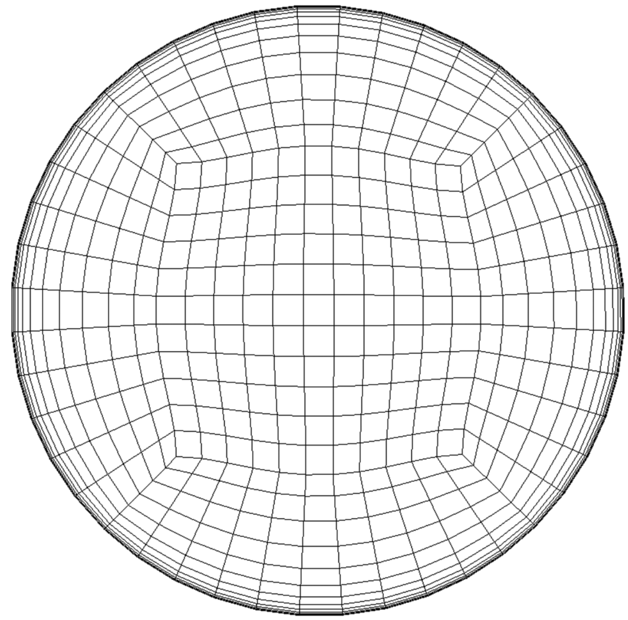

Fig. 3 Grids in the cross-section of the helical tubes

Nu values computed based on the Grid 3 and the Grid 4 is very small. For saving computer resource and keeping a balance between computational economics and accuracy, Grid 3 is adopted in the present simulation.

The time step independence test has been performed based on three time step sizes and they are $\Gamma/50$, $\Gamma/100$ and $\Gamma/200$, respectively. After the flow reaches periodic stability, the results of temperature difference (ΔT) between inlet and outlet with three different time step sizes are shown in Fig. 4. It can be seen that the relative deviation of ΔT in the cases of $\Gamma/100$ and $\Gamma/200$ is less than 0.01%, thus the time step size is set as $\Gamma/100$.

3 Experimental validation

3.1 Experimental setup

In order to test the accuracy of the simulation model and numerical method adopted in the present study, an experiment

Table 3 Variation of f_D and Nu with cell number for the helical tube at $Re = 2982$

	The number of grids	f_D	Nu	Absolute values of relative devation(%)	
Grid 1	1111808	0.09951	25.3535	-	-
Grid 2	1389760	0.09290	25.26407	6.64	0.35
Grid 3	1516352	0.09280	25.25944	0.107	0.018
Grid 4	1683856	0.09276	25.26026	0.043	0.0032

Fig. 4 Time step ΔT independence

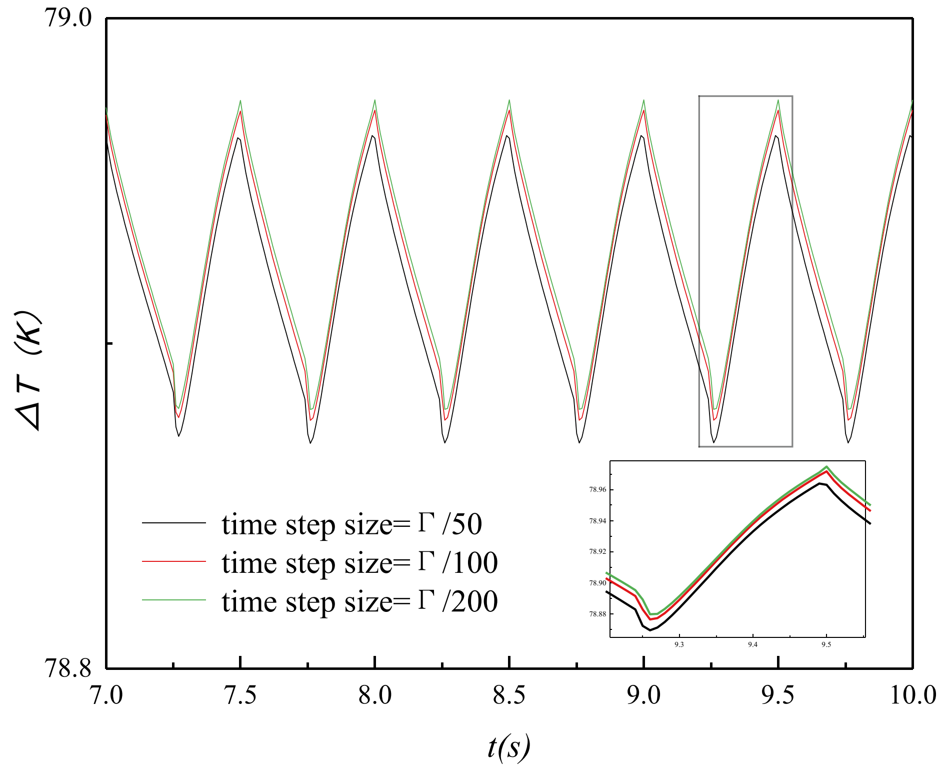

has been carried out on the helical tube. Figure 5 illustrates schematic diagram of experimental setup. The experimental system is mainly composed of pump, helical tube, pulsating device, heating device, measuring instruments, connecting pipes and valves. The helical tube is made of copper. The pulsating flow is generated by a solenoid valve. The time of opening and closing of the solenoid valve is controlled by the time controller to achieve the desired frequency. The heating device is a constant temperature water tank with three electrical heaters. The constant temperature water tank is made of stainless steel. Three electrical heaters and three thermocouples are installed at the bottom of the tank. In order to maintain the ambient hot water temperature at a constant value, the thermocouple is connected with the temperature control switch to control the working state of the heater. The constant temperature tank is also equipped with a circulating pump, which starts automatically when the temperature difference of the three thermocouples exceeds 0.5 K and closes automatically when the temperature difference of the three thermocouples is less than 0.1 K, so that the overall water temperature in the tank is kept at (343 ± 2) K.

Cold water at 20 °C is pumped out of the storage tank and discharged after heat exchange in the test section. In order to ensure the stability of the mainstream flow, a pipeline is

Fig. 5 Schematic diagram of experimental setup

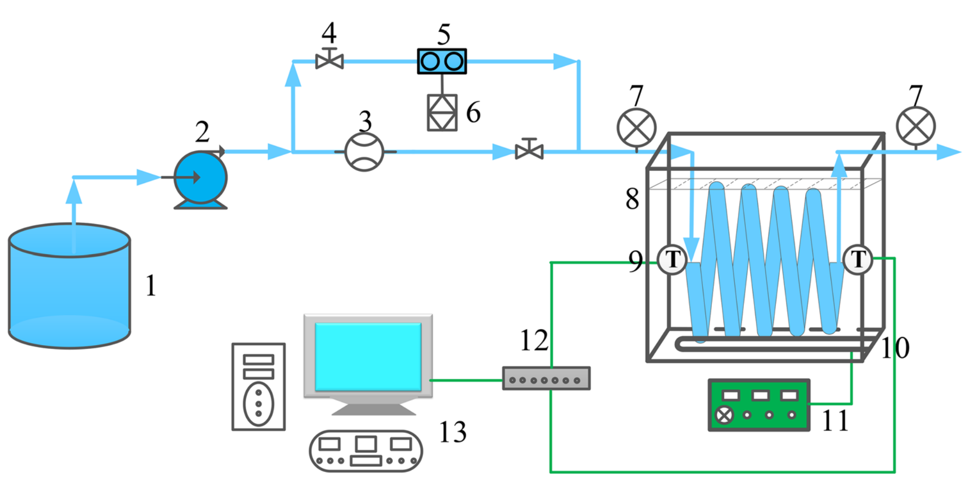

designed in parallel with the pulsating flow. This can also avoid damage to the pipeline in practice. The flowmeter is installed on mainstream pipe to measure flow rate. The valve is used for controlling the flow rate which is positioned at the pulsating device and the parallel pipe. The flow rate is measured by volume flow rate method. Namely, the measuring cylinder measures the liquid collected in a period, and the time is measured by stopwatch. The total flow rates of water ranges from 0.03 to 0.3 cubic meter per hour and the corresponding *Re* number is between 1400 and 8950. The fluid temperature at the inlet and outlet of test section is measured by type-K thermocouples. The temperature is collected by HIOKI (LR8432-30) heat flow meter and saved automatically within 0.5 s intervals, and then the data are transferred to the computer for processing. In order to obtain the pressure drop, two intelligent manometers (JC-80XB) are installed at the inlet and outlet of the helical tube. All parameters are collected and recorded when the system reaches the steady condition. After that, the flow rate changed to the new desired velocity and above procedure is repeated. The same experimental procedure has been independently repeated for three times to assess the reproducibility and reliability.

3.2 Experimental uncertainty

The uncertainty of the above experiments is analyzed, based on the equations presented by Kline and McClintock [32]:

$$R = R(x_1, x_2, ..., x_J) \cdots U_R = \sqrt{\sum_{i=1}^{J} \left(\frac{\partial R}{\partial x_i} U_i \right)^2} \tag{14}$$

where, U_R and U_i are the uncertainties for the results and the independent variables, respectively. The accuracy of measuring instruments and uncertainty of calculated variables are presented in Table 4. For all experimental runs, the maximum uncertainties of *Nu* and f_D are about 8.8% and 9.3%, respectively.

3.3 Comparison of simulated and experimental results

Figure 6 shows the comparison of simulated and experimental values of *Nu* and f_D. The uncertainty bars are indicated on the experimental data. Based on experimental values, the average values of relative deviation of *Nu* and f_D are 8.51% and 8.97%, respectively for the pulsating flow. The agreements between the numerical and experimental results are acceptable. This illustrates that the calculation model and numerical method in the present study are feasible and the simulated results are reliable.

Table 4 Measuring instruments accuracy

Measured parameter	Instrument	Accuracy
Tube	Vernier caliper	±0.02 mm
Volume	Measuring cylinder	±0.01 L
Time	Stopwatch	±0.3 s
Flow rate	flowmeter	±0.5% F.S
Temperature	K-type thermocouple	±0.5 °C
Pressure	Intelligent manometer	±0.2% F.S

4 Results and discussions

4.1 Effects of pulsating parameters

Figure 7 presents the effects of *Wo* number on *Nu* and f_D at $\overline{A} = 0.5$. In the present study, the pulsating frequency f of the square wave pulsating flow is in the range of 0.125 Hz-8 Hz and the corresponding calculated *Wo* number is between 3–27. The average flow rate of helical tube in pulsating flow state is the same as that in steady flow state for comparison. It can be seen from Fig. 7 that both *Nu* and f_D values under pulsating flow are greater than those under steady flow ($Wo = 0$) at the same *De* number. This illustrates that the square wave pulsating flow can further improve the heat transfer performance of the helical tube, however, it will increase the flow resistance. Computed results show that compared with the steady flow, *Nu* is increased by 11.0% on average, and f_D is increased by 9.22% on average in the pulsating state.

It is worth noting that in pulsating state, the effect of *Wo* on *Nu* is more significant at high *De* number. This is mainly because the heat transfer enhancing of helical tubes mainly depend on the action of secondary flow. The existing research results [16] show that the secondary flow plays a primary role in heat transfer enhancement at low *Re* number or *De* number. With the increase of *Re* number, the location of secondary flow gradually approaches the outer wall, which reduces its contribution to enhanced heat transfer. It is pointed out in the literature [33] that when the Reynolds number increases to a certain value, the heat transfer effect of the helical tube is equivalent to that of the straight tube. At this time, the heat transfer performance mainly depends on the turbulence intensity of the fluid. In the present study, the curvature of the helical tube remains unchanged and the increases of *De* number mean increases of *Re* number. In the case of small *De* number, increasing the frequency of pulsating flow cannot significantly improve the intensity of secondary flow, so the effect of heat transfer enhancement is not obvious. However, the flow resistance coefficient increases significantly due to the increase of disturbance. Under the condition of high *De* number, the larger the pulsating frequency *Wo* is, the easier it is to enhance the turbulence intensity of the fluid and improve the heat transfer performance.

Fig. 6 Comparisons between the numerical results and the experimental results at $Wo = 9$ and $\overline{A} = 0.5$

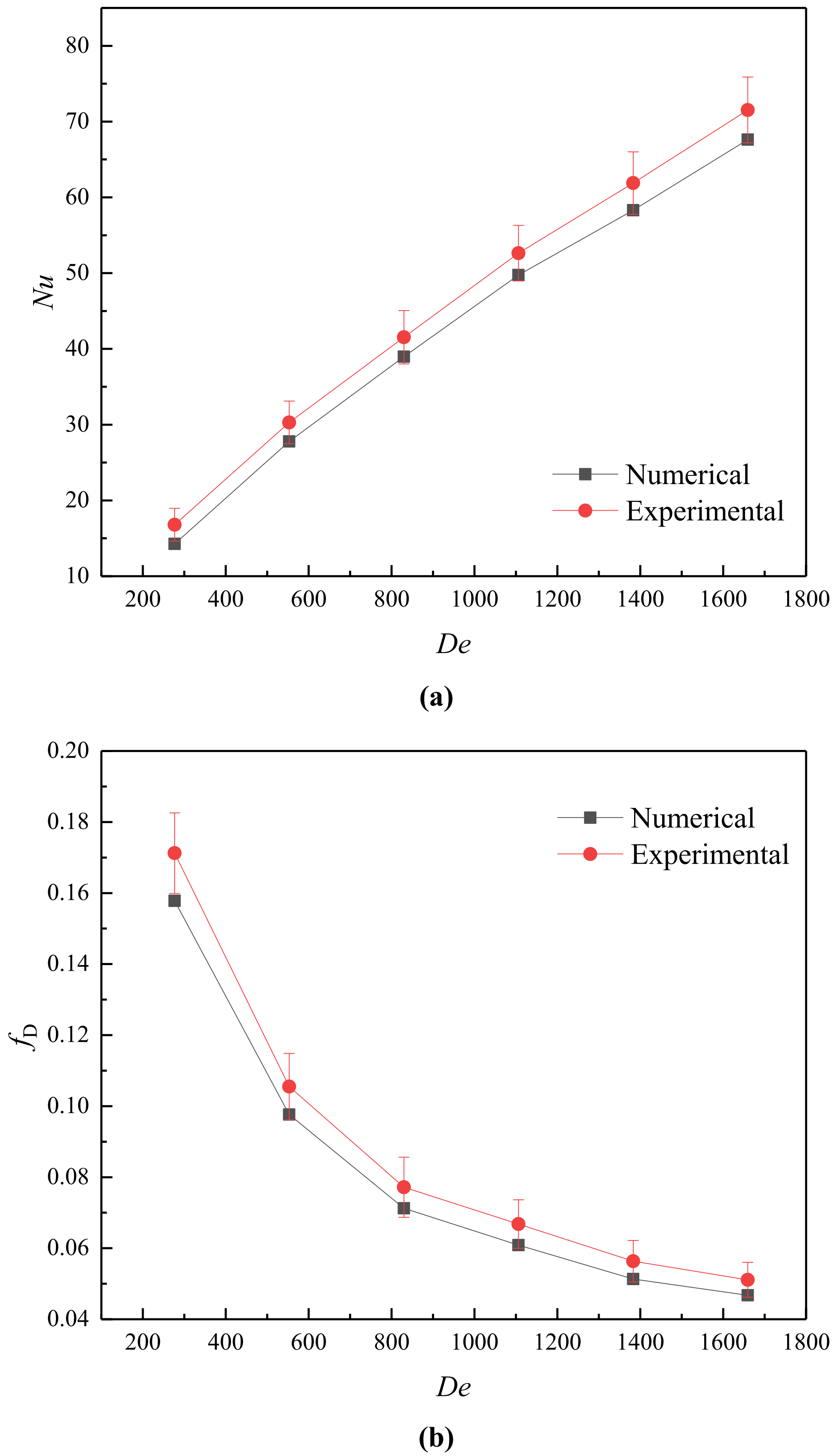

Fig. 7 The variations of Nu and f_D with Wo at $\overline{A}=0.5$

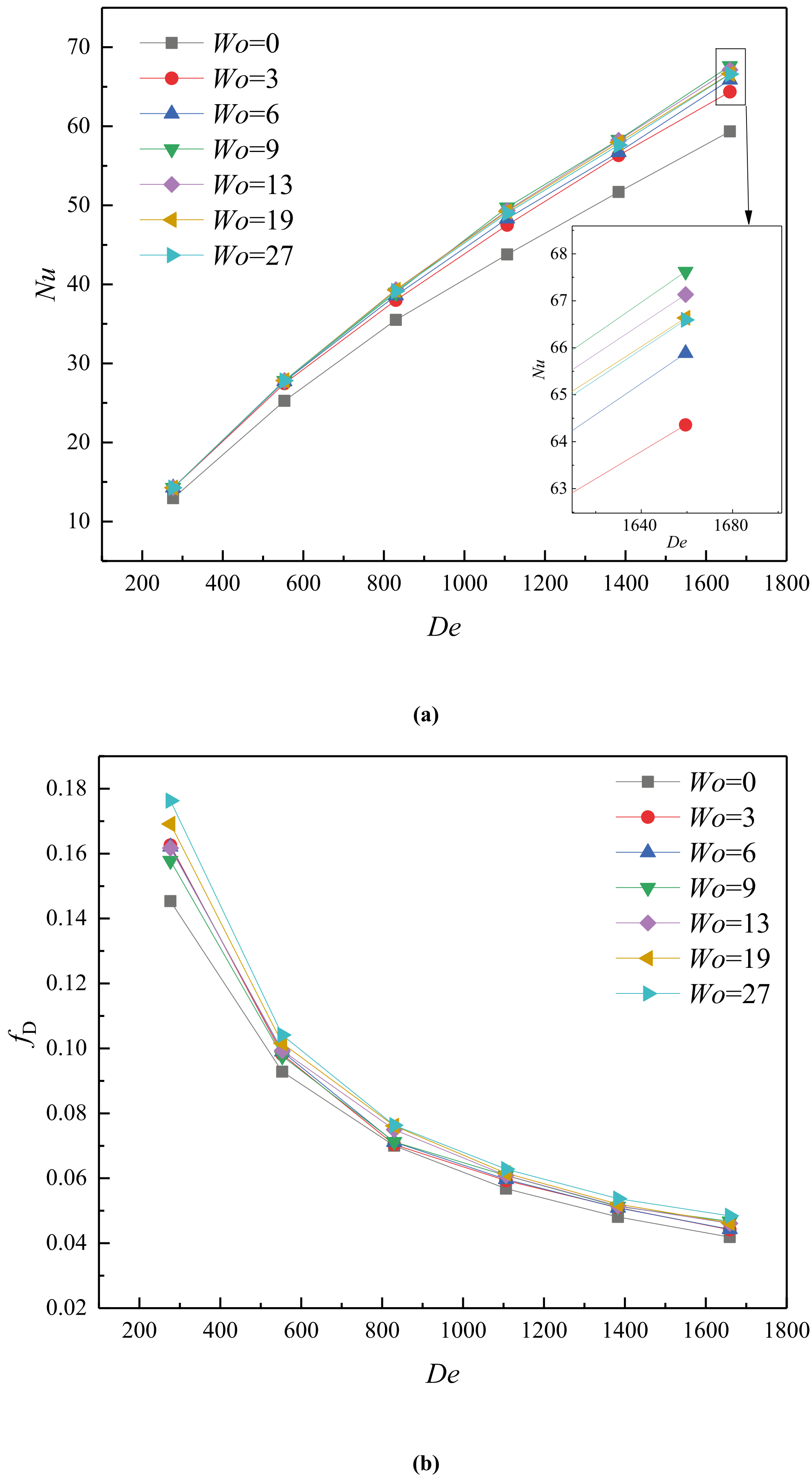

Fig. 8 The variations of *TP* with *Wo* at $\overline{A}=0.5$

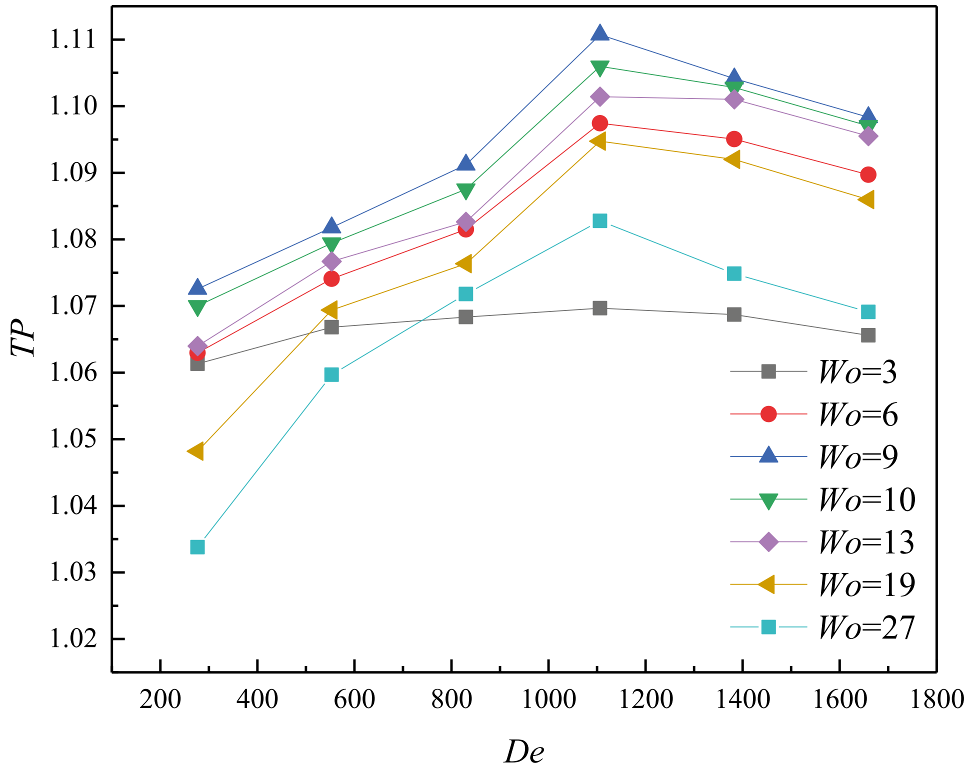

In order to evaluate the comprehensive heat transfer enhancing performance of square wave pulsating flow in the helical tube, comprehensive enhancement heat transfer factor *TP* is adopted and is defined as [34]:.

$$TP=\left(\frac{Nu_{\mathrm{p}}}{Nu_{s}}\right)\cdot\left(\frac{f_{\mathrm{D,p}}}{f_{\mathrm{D,s}}}\right)^{-1/3} \tag{15}$$

where, Nu_{p} and $f_{\mathrm{D,p}}$ is the values in the pulsating state. Nu_{s} and $f_{\mathrm{D,s}}$ is the values in the steady flow state with the same average flow rate.

Figure 8 displays the variations of *TP* values against *Wo*. It can be seen that *TP* values are all greater than unity in the studied scope, which illustrate that it is significant to use square wave pulsating flow to enhance fluid heat transfer in helical tubes. It can also be observed that case of $Wo=9$ is optimal in the studied range. When *Wo* is greater than 9, the *TP* value decreases gradually. This is for the reason that the improvement and development of the secondary flow not only contribute to heat transfer enhancement but increase the flow resistance under the pulsating flow condition. Only the optimal pulsating frequency can appropriately balance the relation between the generation, the growth and the expansion of the vortex so as to obtain the sufficient mixing of the fluid as well as the best heat transfer enhancement effect [26]. The results shows that *TP* values is in the range of 1.03–1.11 at the case of $Wo=9$.

Figure 9 presents the effects of $\overline{A}$ on *Nu* and f_{D} at $Wo=9$. It can be found that similar to the effect of *Wo*, an increase in $\overline{A}$ values also leads to the increase in *Nu* and f_{D}. This is for the reason of the larger the pulsating amplitude, the stronger ability is of disturbing and mixing the fluid. This benefits to the heat transfer enhancement but makes the flow resistance increase at the same time. Figure 10 displayed the variations of *TP* values against $\overline{A}$. It can be found that *TP* increases at first and then decreases with the increase of $\overline{A}$. When $\overline{A}$ is greater than 0.25, the *TP* value decreases gradually, and especially *TP* value decreases more obviously under the condition of low *De* numbers than that of high *De* numbers. This illustrates that the increase amplitude of flow resistance is greater than that of heat transfer with the increase of $\overline{A}$. There is an optimum *De* number $De=1106$ at which the *TP* value obtains maximum. The optimal value of dimensionless amplitude is $\overline{A}=0.25$. Computed results show that *TP* values is in the range of 1.04–1.12 at $\overline{A}=0.25$ and $Wo=9$.

4.2 Heat transfer enhancement mechanism

4.2.1 Flow and temperature fields

The characteristic of square wave pulsating flow different from the steady flow is that there are two times of abrupt velocity changes in one pulsating period. One is at the beginning of the period and the other is in the middle of

Fig. 9 The variations of Nu and f_D with $\overline{A}$ at $Wo=9$

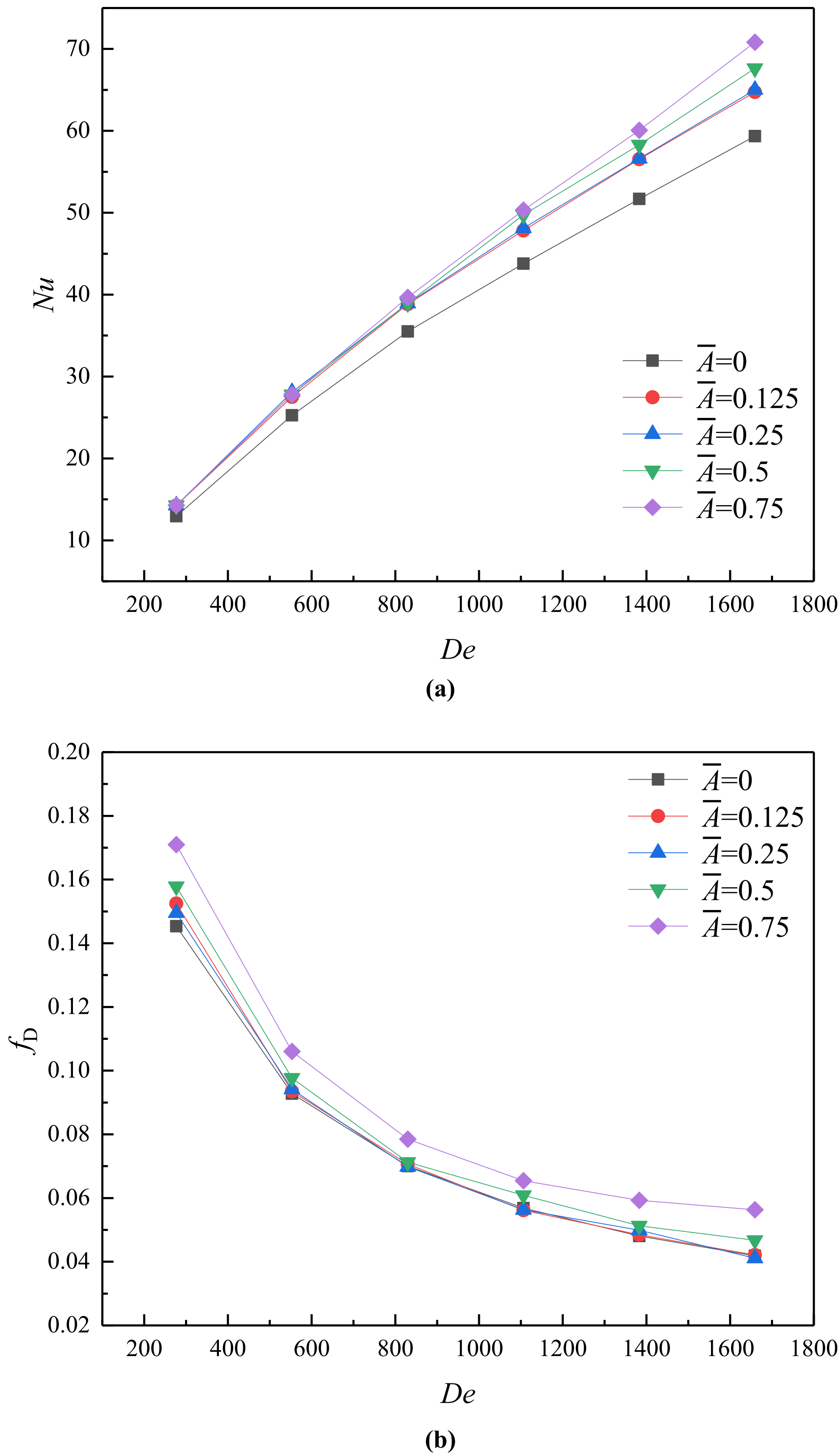

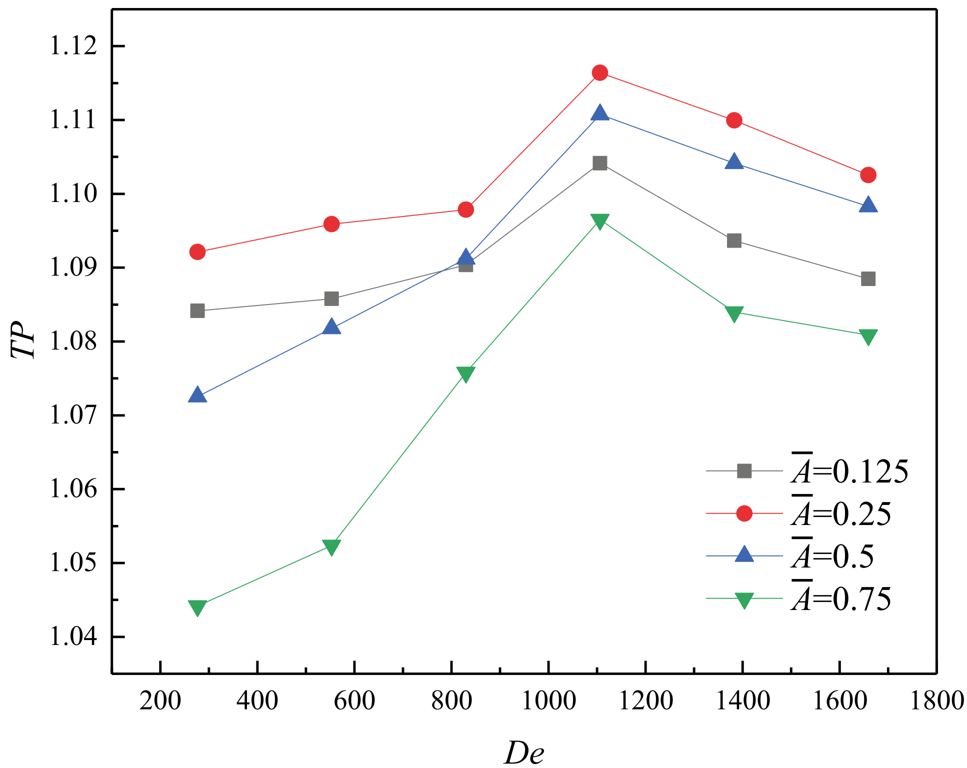

Fig. 10 The variations of TP with $\overline{A}$ at $Wo=9$

the period. The sudden increase or decrease of velocity will change the original flow fields in helical tubes, and then affect the convection heat transfer performance. In order to reveal the heat transfer enhancement mechanism of square wave pulsating flow in helical tube, flow and temperature fields in one pulsating period have been discussed in detailed. The cross section of $\alpha=720°$ is selected and the flow parameters are $De=1106$, $Wo=9$ and $\overline{A}=0.25$.

Figure 11 gives the contour of instantaneous dimensionless temperature $\overline{T}=(T_m\text{-}T_w)/(T\text{-}T_w)$ and dimensionless tangential velocity $\overline{v}_\theta=v_\theta/v_m$ in the cross section of one pulsating period. T_m is the average temperature of cross section. Here, the right of the cross section is the outer wall of the helical tube. Figure 12 gives the change of dimensionless tangential velocity $\overline{v}_\theta$ distribution on the centerline of the cross section during one pulsating period. From the two figures it can be found that the location of the maximum values of $\overline{v}_\theta$ is near the outer wall in the cross section. This phenomenon occurs due to the effect centrifugal force. The tangential velocity gradient and the temperature gradient near the outer wall of

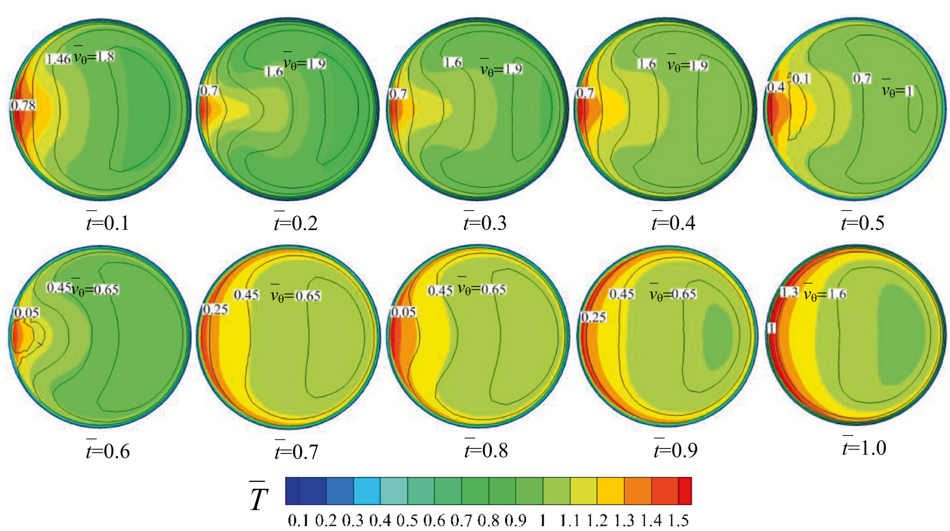

Fig. 11 The distribution of $\overline{T}$ and $\overline{v}_\theta$ in a pulsating period at $\alpha=720°$ for $De=1106$, $Wo=9$ and $\overline{A}=0.25$

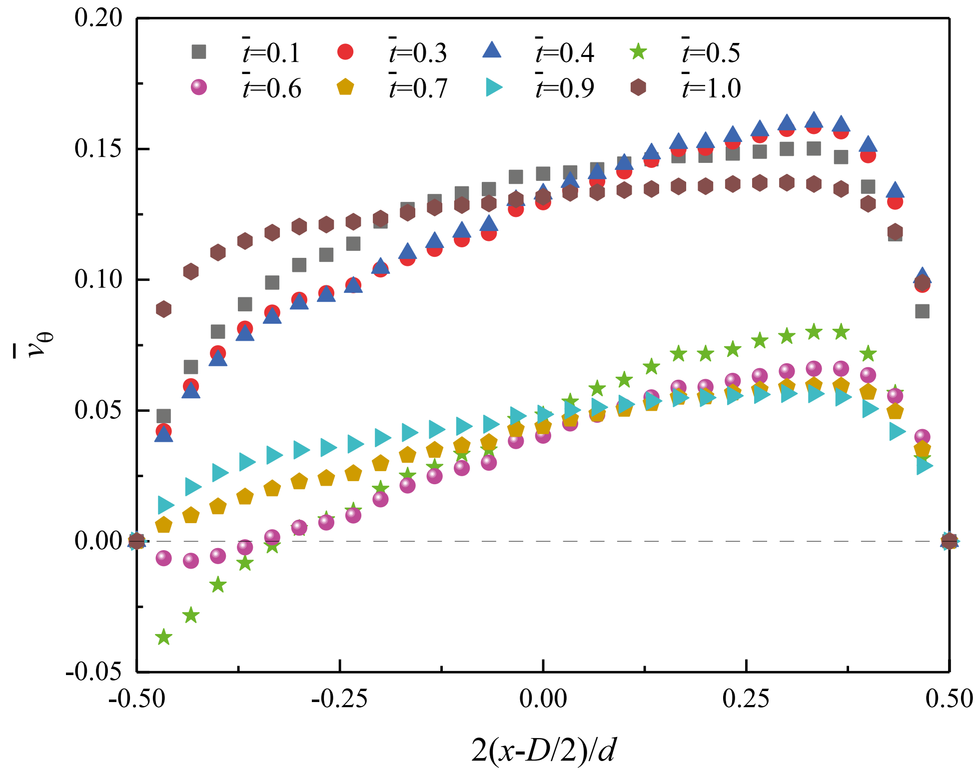

Fig. 12 The distribution of $\overline{v}_\theta$ on the centerline of the cross section of $\alpha = 720°$ during one pulsating period at $De = 1106$, $Wo = 9$ and $\overline{A} = 0.25$

the cross section are both greater than those near the inner wall at any moment. Therefore, the heat transfer capacity of the outer wall is better than that of the inner in helical tubes under the pulsating flow condition, which is similar with that under the steady flow condition. It can also be found from the two figures that the velocity field is more uneven around the time when the velocity changes suddenly. On the contrary, the temperature distribution in the cross section tends to be more uniform except the location near the inner wall. This indicates that the sudden change of velocity of the pulsating flow is beneficial to promote the mixing of the fluid in the helical tube and enhance the heat transfer performance. It is worth noting from Fig. 12 that the values of $\overline{v}_\theta$ near the inner wall is negative at the time of $\overline{t} = 0.5$ and $\overline{t} = 0.6$. This illustrates that there is a backflow at the end of half period due to the sharp reduction of flow rate. The appearance of reflux near the inner wall also contributes to the enhancement of heat transfer.

It is well known that the intensity and scope of secondary flow directly affect the heat transfer performance of the helical tube. The distributions of the time-average dimensionless vorticity magnitude of secondary flow during one pulsating period have been shown in Fig. 13. It can be deduced

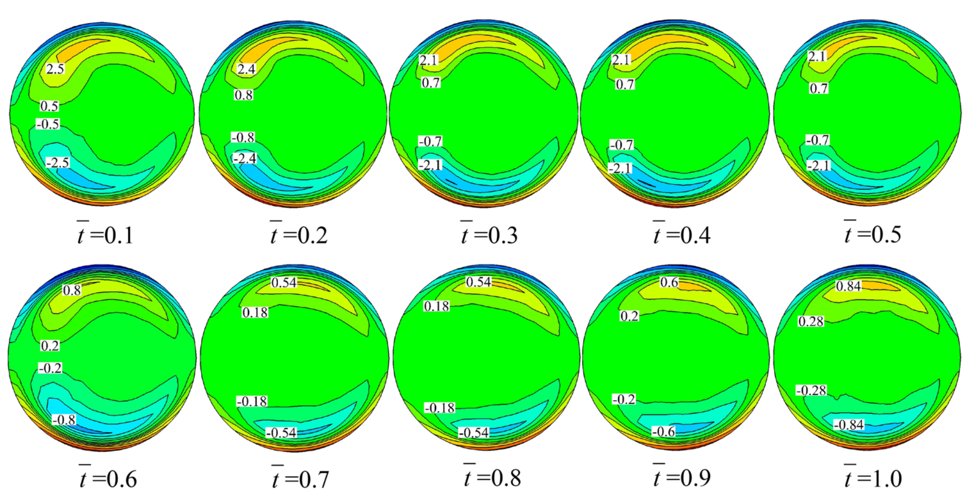

Fig. 13 The distribution of the time-average dimensionless vorticity magnitude on the cross section of $\alpha = 720°$ during one pulsating period at $De = 1106, Wo = 9$ and $\overline{A} = 0.25$

that there is mainly one pair of symmetrical vortices of secondary flow in the cross section. Define the time segment between $\bar{t}=0.1–0.5$ as high flow rate time period and that between $\bar{t}=0.6–1.0$ as low flow rate time period. It can be seen that the vorticity of the former period is higher than that of the latter due to the great flow rate. Moreover, the intensity of secondary flow increases when the flow changes suddenly. This shows that the square wave pulsating flow can further enhance the strength of secondary flow in the helical tube.

4.2.2 Local enhanced heat transfer characteristics

Figure 14 has displayed the distribution of local Nusselt number Nu_{local} along the circumference of wall of the cross section both in steady and pulsating state. It can be seen that under the influence of the flow field, the Nu_{local} values near the outer wall of the helical tubes is significantly higher than those near the inner wall in the two flow states. It shows that the heat transfer near the inner wall of the helical tube is inefficient. The Nu_{local} values in the pulsating state are greater than the corresponding values in the steady state. This is mainly because the pulsating flow not only increases the turbulent ability of the fluid, but also enhances the intensity of the secondary flow. It can also be observed that values of Nu_{local} near the outer wall at $\bar{t}=0.1$ are higher than those at $\bar{t}=0.6$ due to the greater flow rate. However, Nu_{local} values near the inner wall at $\bar{t}=0.6$ is greater than the corresponding values at $\bar{t}=0.1$ although the flow rate at this time is smaller. This may be due to the backflow at the inner wall when the flow suddenly decreases.

Define the average value of Nu_{local} on the heated wall is as $(Nu_{\mathrm{local}})_{\mathrm{m}}$. Figure 15 gives the change of $(Nu_{\mathrm{local}})_{\mathrm{m}}$ with

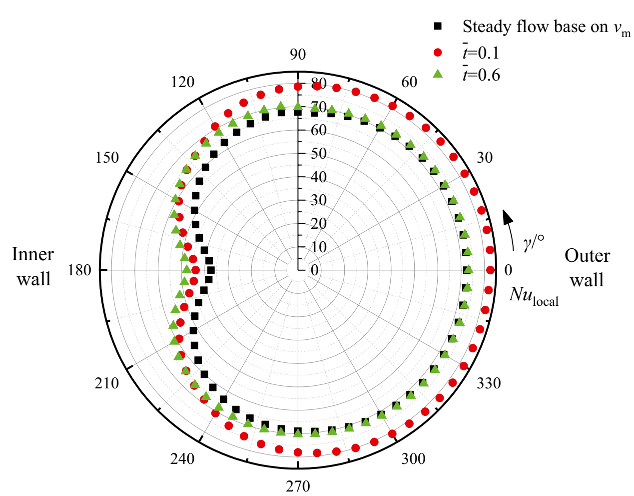

Fig. 14 Distribution of Nu_{local} on the circular wall at $\alpha=720°$ for $De=1106$, $Wo=9$ and $\bar{A}=0.25$

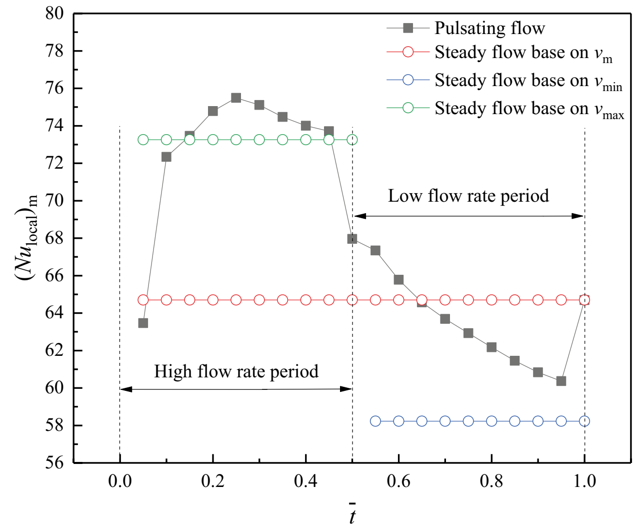

Fig. 15 The average Nu number of the cross section wall during one pulsating period at α=720°, $De=1106$, $Wo=9$ and $\bar{A}=0.25$

time in one pulsating period at $\alpha=720°$. It can be found that in the pulsating state, the $(Nu_{\mathrm{local}})_{\mathrm{m}}$ values in the high flow period are higher than those values in the steady state which are computed based on the maximum velocity v_{max}. Similarly, during the low flow period, the $(Nu_{\mathrm{local}})_{\mathrm{m}}$ values are higher than those values in the steady state which are computed based on the minimum velocity v_{min}. In particular, at the initial time of the low flow rate period, the $(Nu_{\mathrm{local}})_{\mathrm{m}}$ value is even higher than the steady state value calculated based on the average velocity v_{m}. The above results show that the square wave pulsating flow can enhance the fluid heat transfer in the helical tube mainly due to two points: one is the enhancement of the intensity of the secondary flow and turbulence, and the other is the emergence of back flow at the inner wall when the velocity suddenly decreases.

4.2.3 Field synergy mechanism analysis

Field synergy principle is used to further reveal the mechanism of square wave pulsating flow enhancing heat transfer in helical tubes. It has been pointed out by Tao and co-workers [35–37] that the reduction of the intersection angle between velocity vector and temperature gradient can effectively enhance convective heat transfer. The intersection level of the synergy between the temperature gradient and the velocity vector can be expressed by synergy angle θ and it is defined as [38]:

$$\theta = \arccos\left(\frac{\overline{U}\cdot\nabla\overline{T}}{\left|\overline{U}\right|\left|\nabla\overline{T}\right|}\right) \tag{16}$$

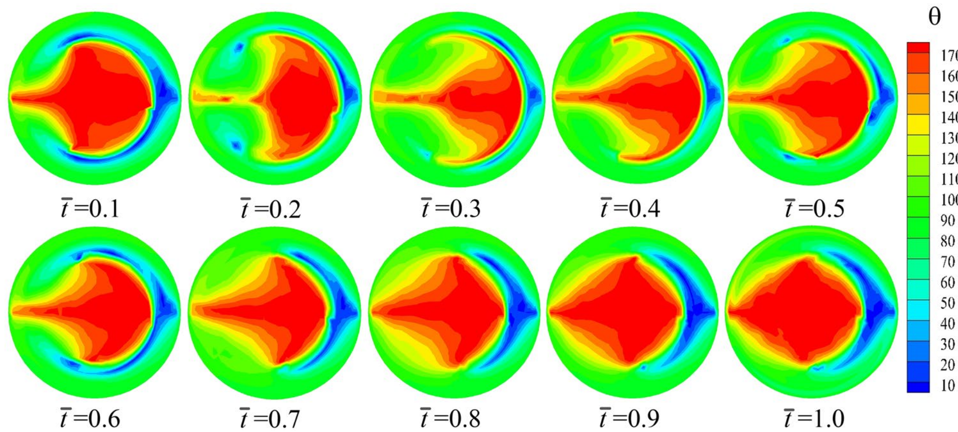

Fig. 16 The average field synergy angle of the cross section of $\alpha = 720°$ during one pulsating period at $De = 1106$, $Wo = 9$ and $\overline{A} = 0.25$

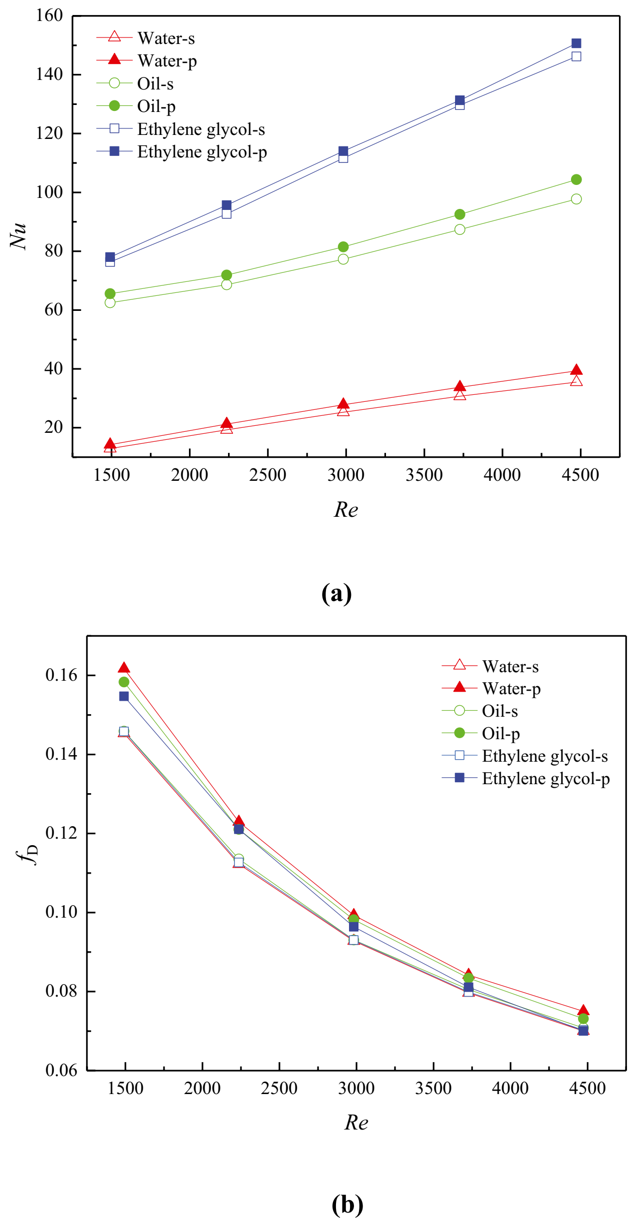

Fig. 17 The variation of Nu and f_D for helical tubes with different working fluids at $Wo = 13$ and $\overline{A} = 0.5$

Here $\overline{\boldsymbol{U}}$ and $\nabla\overline{T}$ are the dimensionless secondary flow velocity vector and temperature gradient, respectively. Figure 16 displayed the distribution of θ in the cross section of $\alpha = 720°$ at $De = 1106$, $Wo = 9$ and $\overline{A} = 0.25$. It can be seen that θ values decrease obviously when the velocity changes suddenly in one pulsating period, which indicates convection heat transfer enhancing.

4.3 Effects of fluids properties

Some studies have reported the effect of Prandtl Number Pr of fluid on heat transfer characteristic in helical tubes under the steady flow condition, but there is no relevant research on the pulsating flow state. Considering this, the oil of $Pr = 50.41$ and ethylene–glycol of $Pr = 150.46$ have been selected as the medium for comparison with water.

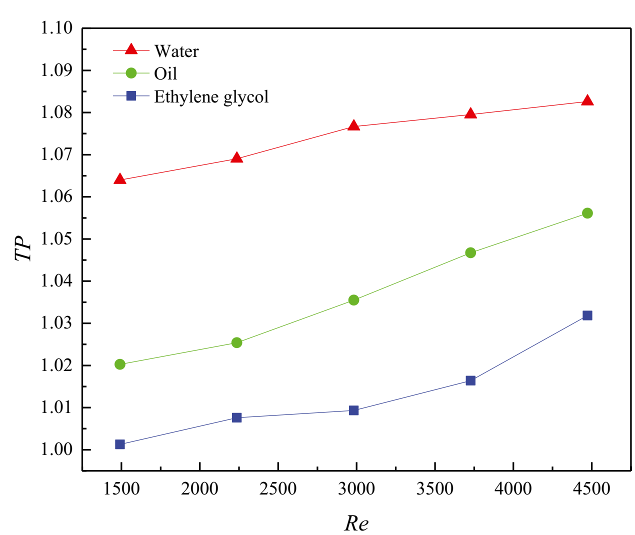

Fig. 18 The variation of TP for helical tubes with different working fluids at $Wo = 13$ and $\overline{A} = 0.5$

Figure 17 gives the effect of *Pr* number on *Nu* and f_D values in the helical tubes under pulsating flow condition. It can be found that in steady flow state, *Nu* is enhanced significantly as *Pr* increases, but the increase amplitude of f_D is small. The similar conclusions can be found in the literature [6]. In the pulsating flow state, both *Nu* and f_D values are enhanced as *Re* number increases. Computed results show that compared with the steady flow, *Nu* of three type of medium in the pulsating flow is increased by 10.3%, 5.6% and 2.3%, however, f_D increased by 8.6%, 6.0% and 31.0% on average, respectively. This lead to *TP* values decreases with the increase of *Pr* number, seen in Fig. 18. Thus the conclusion can be drawn that the fluid of low *Pr* number is more suitable for heat transfer enhancement of square wave pulsating in helical tubes.

5 Conclusions

The square wave pulsating flow is used to enhance convection heat transfer in a helical tube. The influences of dimensionless frequency *Wo*, dimensionless amplitude $\overline{A}$ of the pulsating flow and the Prandtl Number *Pr* of fluid have been discussed in detailed. The heat transfer enhancement mechanism has been revealed. The major conclusions can be drawn as follows.

- Square wave pulsating flow can significantly improve the heat transfer performance of the helical tube. Both *Nu* and *f* values increase as *Wo* and $\overline{A}$ increase.
- The optimum condition of square wave pulsating flow is $Wo = 9$ and $\overline{A} = 0.25$ based which the comprehensive heat transfer enhancement factor *TP* is within the scope of 1.03–1.12 in the studied range.
- Both increase in secondary flow intensity and turbulence intensity as well as the emergence of the backflow near the inner wall contribute to the heat transfer enhancement of square wave pulsating flow in the helical tube.
- Square wave pulsating flow is more suitable for enhancing heat transfer of fluid with small *Pr* number in the helical tube.

Funding This work was supported by the National Natural Science Foundation of China (Grant Nos. 51506133), Natural Science Foundation of Liaoning Province of China (2019MS259) and Foundation of Liaoning Educational Committee (Grant No. LJ2020037).

Declarations

Competing interests Authors are required to disclose financial or non-financial interests that are directly or indirectly related to the work submitted for publication.

References

1. Wang ML, Zheng MG, Chao MK (2019) Experimental and CFD estimation of single-phase heat transfer in helically coiled tubes. Prog Nucl Energy 112:185–190
2. Zhang L, Guo HM, Wu JH, Du WJ (2012) Compound heat transfer enhancement for shell side of double-pipe heat exchanger by helical fins and vortex generators [J]. Heat Mass Transf 48(7):1113–1124
3. Zhang L, Shang BJ, Meng HB, Li YX, Wang CH, Gong B, Wu JH (2017) Effects of the arrangement of triangle-winglet-pair vortex generators on heat transfer performance of the shell side of a double-pipe heat exchanger enhanced by helical fins [J]. Heat Mass Transf 53(1):127–139
4. Yang G, Dong ZF, Ebadian MA (1995) Laminar forced convection in a helicoidal pipe with finite pitch. Int J Heat Mass Transf 38(5):853–862
5. Yang G, Ebadian MA (1996) Turbulent forced convection in a helicoidal pipe with substantial pitch. Int J Heat Mass Transf 39:2015–2022
6. Khoshvaght-Aliabadi M, Tavasoli M, Hormozi F (2015) Comparative analysis on thermal–hydraulic performance of curved tubes: Different geometrical parameters and working fluids. Energy 91:588–600
7. El-Genk MS, Schriener TM (2017) A review and correlations for convection heat transfer and pressure losses in toroidal and helically coiled tubes. Heat Transfer Eng 38(5):447–474
8. Hardik BK, Baburajan PK, Prabhu SV (2015) Local heat transfer coefficient in helical coils with single phase flow. Int J Heat Mass Transfer 89:522–538
9. Li YX, Wu JH, Zhang L (2011) Comparison of fluid flow and heat transfer behavior in outer and inner half coil jackets and field synergy analysis. Appl Therm Eng 31:3078–3083
10. Zhang L, Li JQ, Li YX, Wu JH (2014) Field synergy analysis for helical ducts with rectangular cross section. Int J Heat Mass Transf 75:245–261
11. Li YX, Wu JH, Wang H et al (2012) Fluid Flow and Heat Transfer Characteristics in Helical Tubes Cooperating with Spiral Corrugation. Energy Procedia 17:791–800
12. Zachár A (2010) Analysis of coiled-tube heat exchangers to improve heat transfer rate with spirally corrugated wall. Int J Heat Mass Transf 53(19):3928–3939
13. Rainieri S, Bozzoli F, Cattani L, Pagliarini G (2013) Compound convective heat transfer enhancement in helically coiled wall corrugated tubes. Int J Heat Mass Transf 59:353–362
14. Rainieri S, Bozzoli F, Pagliarini G (2012) Experimental investigation on the convective heat transfer in straight and coiled corrugated tubes for highly viscous fluids: preliminary results [J]. Int J Heat Mass Transf 55:498–504
15. Gholamalizadeh E, Hosseini E, Jamnani MB, Amiri A, Dehghan saeee A, Alimoradi A (2019) Study of intensification of the heat transfer in helically coiled tube heat exchangers via coiled wire inserts, Int J Therm Sci 141:72–83
16. Li YX, Wang X, Zhang J et al (2019) Comparison and analysis of the arrangement of delta winglet pair vortex generators in a half coiled jacket for heat transfer enhancement [J]. Int J Heat Mass Transf 129:287–298
17. Abdelatief MA, Sayed Ahmed SA, Mesalhy OM (2018) Experimental and numerical study on thermal-hydraulic performance of wing-shaped-tubes-bundle equipped with winglet vortex generators [J]. Heat Mass Transf 54(3):727–744
18. Zeeshan M, Nath S, Bhanja D (2020) Numerical analysis to predict the optimum configuration of fin and tube heat exchanger with rectangular vortex generators for enhanced thermohydraulic performance [J]. Heat Mass Transf 56(7):2159–2169

19. Guo LJ, Chen XJ, Feng ZP, Bai BF (1998) Transient convective heat transfer in a helical coiled tube with pulsatile fully developed turbulent flow. Int J Heat Mass Transf 41(19):2867–2875
20. Guo LJ, Feng ZP, Chen XJ (2002) Transient convective heat transfer of steam–water two-phase flow in a helical tube under pressure drop type oscillations. Int J Heat Mass Transf 45(3):533–542
21. Rabadi NJ, Chow J, Simon HA (1982) Heat transfer in curved tubes with pulsating flow. Int J Heat Mass Transf 25(2):195–203
22. Pan C, Zhou Y, Wang J (2014) CFD study of heat transfer for oscillating flow in helically coiled tube heat-exchanger. Comput Chem Eng 69:59–65
23. Pan C, Zhang T, Wang J, Zhou Y (2018) CFD study of heat transfer and pressure drop for oscillating flow in helical rectangular channel heat exchanger. Int J Therm Sci 129:106–114
24. Kharvani HR, Doshmanziari FI, Zohir AE et al (2016) An experimental investigation of heat transfer in a spiral-coil tube with pulsating turbulent water flow [J]. Heat Mass Transf 52(9):1779–1789
25. Doshmanziari FI, Zohir AE, Kharvani HR, Jalali-Vahid D, Kadivar MR (2016) Characteristics of heat transfer and flow of Al2O3/water nanofluid in a spiral-coil tube for turbulent pulsating flow [J]. Heat Mass Transf 52(7):1305–1320
26. Guo WW, Li GN, Zheng YQ et al (2020) The effect of flow pulsation on Al2O3 nanofluids heat transfer behavior in a helical coil: A numerical analysis [J]. Chem Eng Res Des 156:76–85
27. Ye QH, Zhang YH, Wei JJ (2021) A comprehensive review of pulsating flow on heat transfer enhancement [J]. Appl Therm Eng 196(3):117275
28. Zhang H, Li S, Cheng J, Zheng Z, Li X, Li F (2018) Numerical study on the pulsating effect on heat transfer performance of pseudo-plastic fluid flow in a manifold microchannel heat sink. Appl Therm Eng 129:1092–1105
29. Hamed KB, Abbas A, Amir ZR (2019) Heat transfer enhancement and pressure drop by pulsating flow through helically coiled tube: An experimental study [J]. Appl Therm Eng 160(10):114012
30. Jayakumar JS, Mahajani SM, Mandal JC, Vijayan PK, Rohidas B (2008) Experimental and CFD estimation of heat transfer in helically coiled heat exchangers. Chem Eng Res Des 86(3):221–232
31. Jayakumar JS, Mahajani SM, Mandal JC, Iyer KN, Vijayan PK (2009) CFD analysis of single-phase flows inside helically coiled tubes. Comput Chem Eng 34(4):430–446
32. Kline SJ, McClintock FA (1953) Describing uncertainties in single-sample experiments [J]. Mech Eng 75:3–8
33. Bai B, Guo L, Feng Z et al (1997) Turbulent heat transfer in helical coils [J]. J Chem Ind Eng 48(1):18–23
34. Webb RL (1981) Performance evaluation criteria for use of enhanced heat transfer surfaces in heat exchanger design. Int J Heat Mass Transfer 24(4):715–726
35. Tao WQ, Guo ZY, Wang BX (2002) Field synergy principle for enhancing convective heat transfer-its extension and numerical verifications. Int J Heat Mass Transfer 45:3849–3856
36. Tao WQ, He YL, Wang QW, Qu ZG, Song FQ (2002) A unified analysis on enhancing single phase convective heat transfer with field synergy principle. Int J Heat Mass Transfer 45:4871–4879
37. Tian LT, He YL, Lei YG, Tao WQ (2009) Numerical study of fluid flow and heat transfer in a flat-plate channel with longitudinal vortex generators by applying field synergy principle analysis [J]. Int Commun Heat Mass Transfer 36(2):111–120
38. Guo JF, Huai XL (2016) Numerical investigation of helically coiled tube from the viewpoint of field synergy principle. Appl Therm Eng 98:137–143

Publisher's Note Springer Nature remains neutral with regard to jurisdictional claims in published maps and institutional affiliations.